LINEAR FEATURE IDENTIFICATION AND INFERENCE IN NANO-SCALE IMAGES

ILYA LAVRIK AND BRANI VIDAKOVIC

ABSTRACT. In this paper a novel method for the analysis of straight line alignment of features in the images based on Hough and Wavelet transforms is proposed. The new method is designed to work specifically with nanoscale images, to detect linear structure formed by the atomic lattice.

1. INTRODUCTION

Nanoscale materials (i.e. materials designed on the scale of 10^{-9} meters) have been growing in interest in recent years. This is due to the emergence of nanotechnology as a field of interest in technology and to the miniaturization limitations of current technology. Nanoscale-designed materials promise to have radically different properties than their bulk counterparts. For example, the photoluminescence properties of materials change significantly in nanomaterials. Widely discussed, carbon nanotubes have been either semiconducting or metallic and have vastly improved strength over any bulk carbon.

It is important, then, to be able to characterize the materials being used in order to fully understand the properties that they exhibit. A tool crucial to this characterization and understanding is the Transmission Electron Microscope (TEM). In order to view and understand the arrangements of atoms at an atomic scale, a high resolution transmission electron microscope is necessary. Furthermore, tools helping to analyze the images taken from the microscope could vastly enhance the ability of scientists to understand the phenomena that occur when designed at the nanoscale.

Crystalline materials are made up of atoms in specific sites within unit cells. These attributes of crystalline materials help define the many attributes that the bulk material shows. The size of these unit cells is on the order of only a couple of angstroms (10^{-10} meters) and so imaging them is somewhat of a challenge. This is solved through the use of a TEM in which resolutions up to one angstrom have been achieved. In a nanoscale world, the easy and reliable measurement of these properties of the crystals is vital to the characterization of the materials being used.

Lattice spacing determination in high resolution electron microscope images is a key way in which a material can be characterized and studied. The spacing of unit cells of atoms and the angles that the sides of the unit cells make are both techniques in characterizing a crystalline material. Also interesting are spaces in the crystal where this regularity breaks down. This can symbolize defects in the crystal structure, such as dislocations, point defects, and planar defects. Such defects can have a large impact on the properties of the material. In many cases, it can be difficult to see the presence of nanoscale particles without an aid.

Key words and phrases. Hough transform, wavelets, lattice spacing.

We gratefully acknowledge partial support of this project by the Georgia Institute of Technology Molecular Design Institute, under prime contract N00014-95-1-1116 from the Office of Naval Research. Partial support for this work was also provided by National Security Agency Grant NSA E-24-60R.

The authors gratefully acknowledge the help of Daniel Moore during early stages of this work and for providing the images.

When taking a low magnification, high resolution (500kx, 1.2 angstrom resolution) images, layers of atoms manifest themselves as a series of parallel lines. The separation between these lines can be used to determine the separation between the layers of atoms. This is important in determining several important factors about the material, including the crystallographic orientation and some mechanical properties. Most of the time, these lines are visible to the human eye and currently are measured by hand with a magnifying glass, after the pictures of the specimen have been developed, and after the specimen is no longer in the microscope. More and more, these microscopes have digital cameras installed on them, so the ability to make these measurements immediately, while the specimen is still in the microscope is an extremely useful tool to researchers. Knowing what you have already measured while you are still working on the microscope can lead to better analysis and an easier time of making all of the correct measurements. Moreover the visual scans are not very accurate and often miss hidden crystallographic orientations. Therefore, developing a tool to automate the process of determining the spacing and orientation of the lattice of atoms could be important to the development of the understanding of materials and their properties at the nanoscale.

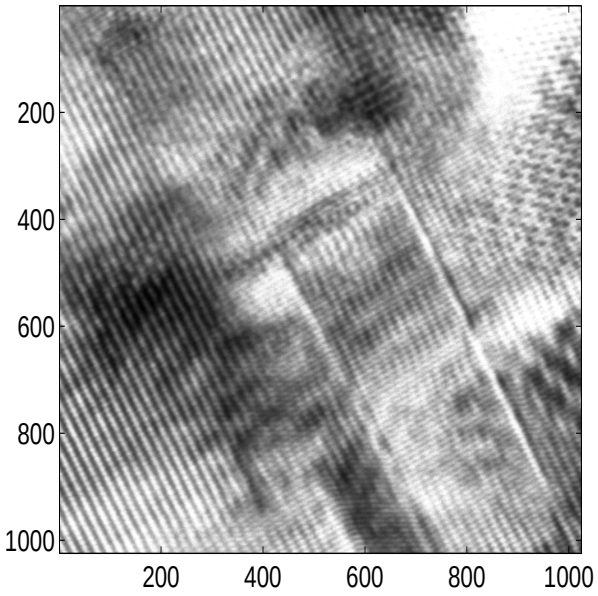

FIGURE 1. Example of the TEM image of the ZnS structure. Parallel lines formed by an atomic lattice are clearly visible. They form approximately 30° angle with the y-axis.

Figure 1, shows the typical TEM image of the ZnS structure. The "linear" structure (parallel lines of different orientation) formed by an atomic lattice is clearly visible. The difference in orientation may come from the following sources: (i) different materials will have different orientation; (ii) often the layer that is below the surface can be seen, and this creates the additional orientation and (iii) different areas of the crystal can be oriented differently. Our primary goal is to detect this linear structure, or more specifically, to find the parallel lines, their relative orientations, and distances between parallel lines of the same direction. All this information is useful in the

following important applications. First of all, by knowing of the relative orientation of different materials we can learn more about the crystallographic structure of the interfaces of the materials. Second, the knowledge of the orientation of the surface layer and the layers below it, coupled with diffraction pattern and images at higher resolution, can give us signature of the material, its structure and properties. Finally by learning the distances between parallel lines the distance between atoms, the lattice spacings can be determined.

This paper is organized as follows. In Section 2 we review concepts from signal and image processing which play an important role in our project. In Section 3 we describe the proposed method. In Section 4 we present the results, and Section 5 is devoted to a discussion.

2. BACKGROUND

The straight lines are the pattern of interest in the images. There are several different ways of representing the straight line in $\mathbb{R}^2$. For convenience, the *normal* representation of the line is used:

$$x\cos\theta + y\sin\theta = \rho,$$

where ρ is the length of a normal from origin to the line and θ is the angle of the orientation of ρ with respect to the x-axis (See Figure 2). Simple geometry shows that the angle between the line and the "negative" y-axis is also θ. In the future, we will refer to an orientation as an angle formed by the line and "negative" y-axis.

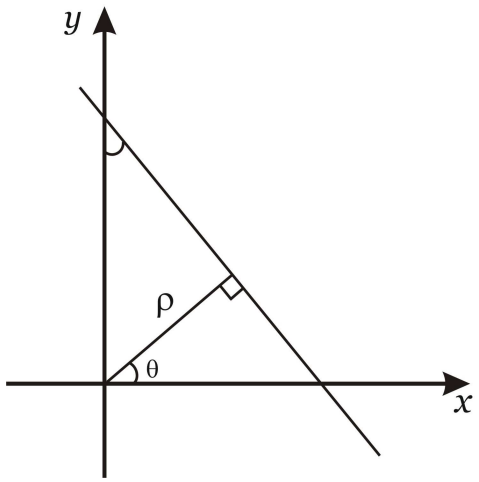

FIGURE 2. Normal representation of a straight line in $\mathbb{R}^2$.

There are many methods in image processing for the detection of lines. One of the most popular is the Hough Transform (HT).

2.1. **The Hough Transform.**

The Hough transform (HT) is a well known tool for the detection of the straight lines. Paul Hough [3], deduced the method in order to detect the straight line tracks left by the charged particles in a bubble chamber. His proposal was based more on intuition than on formal mathematical ground. Later, Duda [2], introduced the (ρ, θ) parametrization, and Deans [1] showed that the Hough transformation is in fact a special case of the well known Radon transform.

The Hough transform involves three main steps. The first step is the computation of a binary edge image $I(x, y)$. The edge description is commonly obtained from a feature detection methods such as the Laplacian of Gaussian method, the zero-crossing method, Robers Cross, Sobel, or

Canny edge detector, and it is usually noisy, i.e. it contains multiple edge fragments corresponding to a single whole feature.

The second step is the evaluation of the formula

$$HT(\rho,\theta) = \iint_{\mathbb{R}^2} I(x,y)\delta(\rho - x\cos\theta - y\sin\theta)dxdy, \tag{1}$$

where δ is the standard delta function, $\delta(x) = 0 \quad \text{for all} \quad x \neq 0$. Equation (1) is the mathematical representation of the standard Hough transform. Any grayscale image is stored in computer as a matrix. Thus function $I(x,y)$ in the Equation (1) will be discrete. This requires the discretization of the the parameters of the lines ρ and θ. Hence the integrals in (1) will be represented as sums. For an $N \times N$ image, discrete values of the (ρ,θ) variables, within the intervals $[-N/\sqrt{2}, N/\sqrt{2}]$ and $[0,\pi]$ respectively. Discretization of the parameter θ may, for example may be from 1 to 180 degrees in steps of $\Delta\theta = 1$, or one may choose half-degree step $\Delta\theta = 0.5$, to increase sensitivity. One can discretize parameter ρ in similar way with different values for the step $\Delta\rho$. The size of the steps creates the dimensions of a "probe line" or rectangular window/band along which the formula is evaluated. Simply stated, the Hough transform computes the sum of the edge map I, along the straight "probe lines" defined by the polar parameters (ρ_n,θ_m), and stores the values in the corresponding bins $HT(\rho_n,\theta_m)$ forming the accumulator matrix R. The Hough transform could be generalized by changing the argument of the delta function. A *generalized* Hough transform can be used for the detection of regular curves such as circles, ellipses, *etc*, and it is can be employed in applications where a simple analytic description of features of a pattern of interest is not possible.

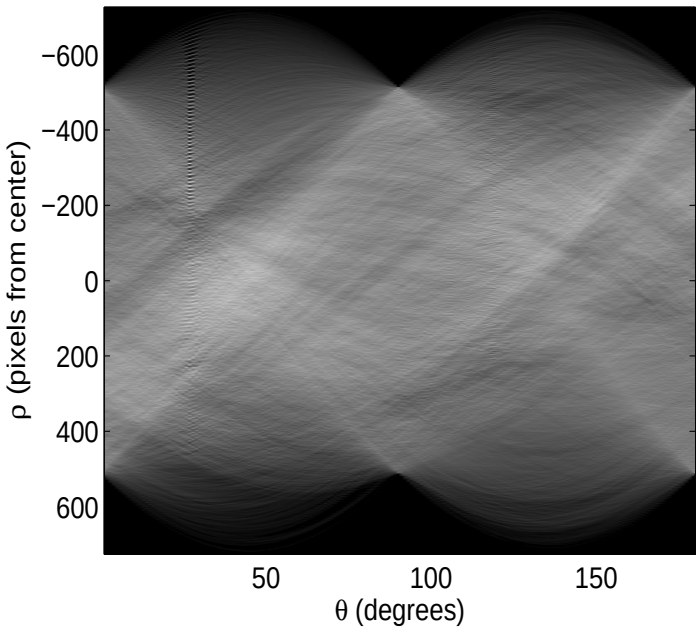

FIGURE 3. Example of the HT applied to image in Fig 1. Notice irregularities at $27°$. These correspond to parallel lines formed by an atomic lattice clearly visible in Fig. 1.

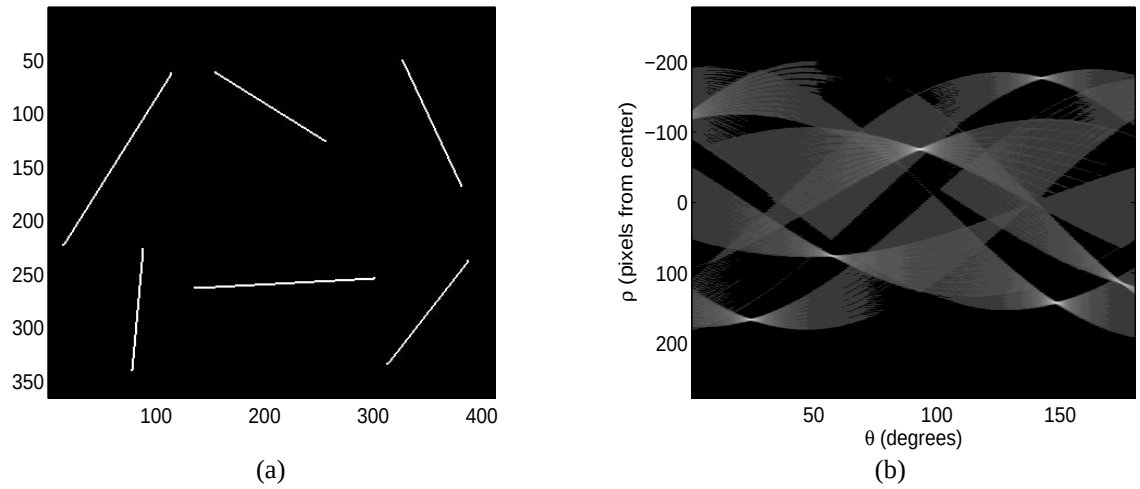

(a) (b)

FIGURE 4. An image with straight lines and the HT of this image. Notice a distinct "butterfly" shape formed by the lines after the HT. The line in the neighborhood of the point $(250, 200)$ which forms an angle slightly over 90° with the y-axis in a) will correspond to the "butterfly" with its center approximately at $(-90, 90)$ in b).

The last step is the analysis of the output. There are number of methods which one can employ in order to extract bright points (*local maxima*), from the accumulator, in other words, unique (ρ, θ) points corresponding to each of the straight lines in the image. The simplest method is the *relative thresholding*. One could take only those local maxima in the accumulator whose values exceed some fixed percentile. However, there are many local maxima that do not correspond to straight lines because of sensitivity of the Hough transform to the correlated noise. Hence, the relative thresholding generally performs poorly.

Figure 4 shows the representation of straight lines in the Hough transform output. The lines have a more complex representation than just the local maxima. One can clearly see the distinct distribution of intensity associated with each straight line featured in image space. The distribution has the appearance of a butterfly with its wings extended in the θ direction. Therefore, instead of looking for local maxima one can be looking for this particular distribution around local maxima. This can be done by using a mask or filter that matches the distribution under investigation. The analytical form of the "butterfly" distribution in transformed space has been deduced using a step by step geometric approach and a limiting process. If the line under detection has a normal which subtends an angle α with the x-axis, then

$$HT(\rho, \theta) = \frac{1}{|\sin(\theta - \alpha)|}.$$

More information about the Hough transform, butterfly distribution and filtering, and other Hough transform techniques can be found in [5] and [4].

2.2. **Wavelets.** Wavelet theory has developed into a methodology that is used in a range of disciplines, including mathematics, physics, geophysics, astronomy, signal processing, statistics, and a number of applied fields. Wavelets provide a rich source of already indispensable and intriguing tools for "time-scale" applications. The success of wavelets is attributed to their low computational complexity, good locality and adaptivity, and potential to incorporate prior information about the

phenomena. Hence, wavelets are natural tools in modeling complex data structures and multiscale phenomena considered in this project. Wavelet-based methods have also proved to be very advantageous for application to various theoretical statistical problems such as regression, probability density estimation or inverse problems.

Wavelets and wavelet-like decompositions are well suited for analysis of non-stationary and non-isotropic phenomena. They are capable of "zooming-in" and exploring local features at various scales of interest. An additional feature of multiscale methods is that they are "friendly" towards large data sets. In fact, fast filtering algorithms needed to perform wavelet transform exceed in speed classical fast fourier transforms (FFT) and have a calculational complexity of $O(n)$.

Wavelets form an orthonormal basis $\{\phi_{j_0,k}, \psi_{j,k}, j \geq j_0, k \in \mathbb{Z}\}$. It is known that any square integrable function $f(x)$ can be decomposed with respect to wavelet basis into the following series

$$f(x) = \sum_k c_{j_0,k}\phi_{j_0,k}(x) + \sum_{j,k} d_{j,k}\psi_{j,k}(x),$$

where

$$c_{j_0,k} = \int f(x)\phi_{j_0,k}(x)dx, \quad d_{j,k} = \int f(x)\psi_{j,k}(x)dx.$$

One of the major specificities of the wavelet orthonormal basis is in the fact that functions $\psi_{j,k}$ and $\phi_{j_0,k}$ can be expressed as a scale-shift transform of functions ψ and ϕ as

$$\psi_{i,j}(x) = 2^{j/2}\psi\left(2^j \cdot x - k\right), \quad \phi_{i,j}(x) = 2^{j/2}\phi\left(2^j \cdot x - k\right).$$

Functions $\psi(x)$ and $\phi(x)$ are called wavelet and scaling functions respectively. The function $\phi(x)$ is different in nature, than the functions $\psi_{j,k}$, $j, k \in \mathbb{Z}$. While the functions $\psi_{j,k}$, describe the details in the decomposition (such as fast decay, oscillations, high frequency features, *etc*) the function $\phi(x)$, is responsible for trend features of the decomposed function. The scaling function satisfies the following relationship

$$\phi(x) = \sum_k h_k\phi(2x - k), \tag{2}$$

leading to fast filtering schemes involving a filter for h_k. Both wavelet and scaling functions can be completely defined by a suitable choice of the coefficients h_k in (2). There are many different families of wavelets designed for capturing various features of the signals under investigation. More information on the wavelets can be found in [7].

3. Method Description

As mentioned above, the first step is the creation of the binary edge map, edge detection. The Canny method of edge detection was found to be particularly well suited for this purpose. The method finds edges by looking for local maxima of the gradient of the image, calculated using the derivative of a Gaussian filter. The method uses two different thresholds. The first threshold detects strong and weak edges, and the other includes the weak edges in the output only if they are connected to strong edges. Compared to other standard methods, the Canny algorithm is less likely to be "fooled" by noise, and is more likely to detect true weak edges.

After the edge detection is complete, the standard Hough transform is performed to obtain the accumulator matrix R. The parallel lines of different orientation formed by the atomic lattice is pattern of interest. Due to the physical nature of the images, the presence of the parallel lines throughout the whole image is expected. Parallel lines with the same orientation will be represented

as bright points at one specific column (equivalently, angle) of the accumulator matrix R. Thus it is expected that some angles would have more energy than that of others. The energy function Ang, can be obtained from the accumulator matrix R, as follows

$$Ang(j) = \sum_i R_{i,j}^2, \quad \text{for} \quad j = 1, 2, \ldots 180.$$

For convenience, Ang is normalized, so that it has a zero mean, and a unit sample variance. Figure 5 illustrates the application of the above concept to the image in Figure 1.

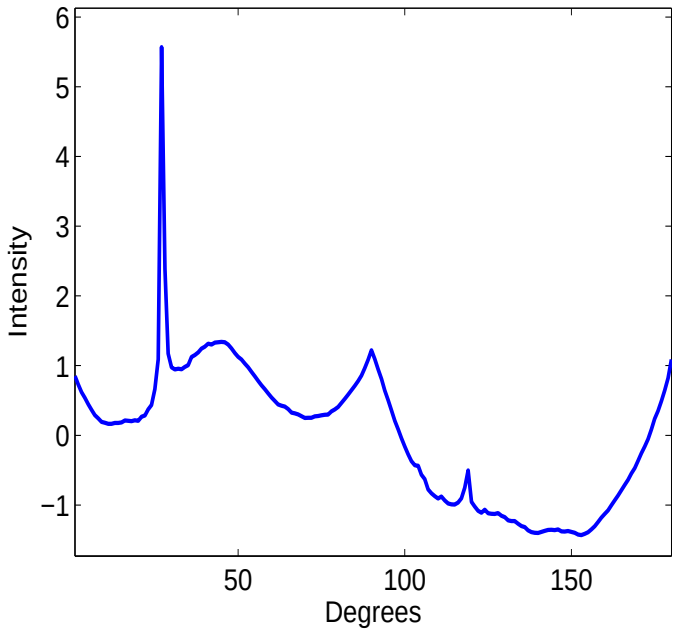

FIGURE 5. Energy plot Ang of the HT accumulator matrix R for the image in Fig. 1. Notice three distinct peaks at $27°$, $90°$ and $119°$. The peak at $27°$ corresponds to a major visible orientation of the image in Fig. 1. The peak at $119°$ corresponds to a second orientation, which is barely visible.

The energy function helps identify the angles that correspond to structured patterns of parallel lines. These angles will be represented on the graph of the energy function as sharp peaks. On the other hand, those that do not correspond to such patterns, for example some instances of correlated noise, will show up as flatter or less sharp local maxima. This behavior is captured in Figure 5, where three distinct peaks can be observed at $27°$, $90°$, and $119°$ elucidating patterns of parallel lines aligned at those angles. There is also a flat local maxima present around $45°$ which does not correspond to a pattern of interest. In this way, the identification of peaks in the graph of the energy would accurately determine the orientations of the parallel lines formed by the atomic lattice.

Because of their localization property, wavelets are employed as an appropriate tool for detecting peaks. To this end, the non-decimated wavelet transform of the energy function Ang is performed using the Haar wavelet. Using two levels of the decomposition has proved to be sufficient to detect the peaks. The coefficients at the two detail levels with large absolute values would correspond to irregularities in the energy function Ang since the levels are close to the first and second discrete derivatives of the function. For the Haar wavelet, if properly scaled, the first two levels are exactly

the first two numerical derivatives. The following rule is used in order to determine the significance of an angle. The angle i, for $i = 1, 2, \ldots 180$, is considered to be a significant if it satisfies:

$$\alpha d_{i,1} + (1-\alpha) d_{i,2} > \alpha q_{p_1}(\text{level1}) + (1-\alpha) q_{p_2}(\text{level2})$$

and

$$d_{i,1} > 0, \quad d_{i+1,1} < 0,$$

where $d_{i,1}$ and $d_{i,2}$ are the coefficients of the first and second levels of the decomposition, respectively, corresponding to a given angle i. The $q_p(\text{level k})$ is the $p \cdot 100\%$ quantile of the coefficients of level k, for $k = 1, 2$. The relative importance of the levels is selected by the value of α. The default values of p_1, p_2, and α are 0.90, 0.75, and 0.75, respectively. These default parameters provide very good results in noisy and real life images. These parameters can be changed in order to increase sensitivity and detect otherwise overlooked features. The first expression in this rule finds all significant coefficients in the decomposition which correspond to irregularities in the function Ang such as fast decay, discontinuity jumps, peaks, *etc*. The second guaranties that the suspicious angle is local maxima. This rule proves to be a very efficient in finding peaks of the function Ang.

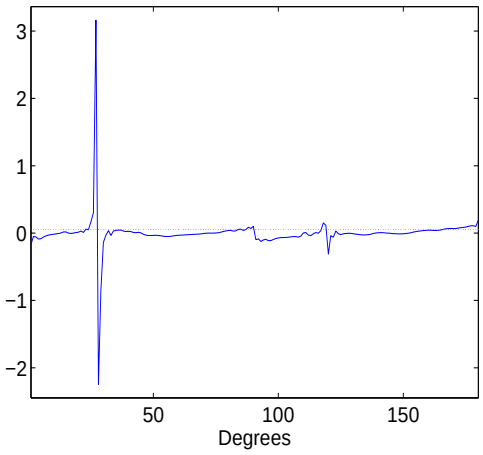

FIGURE 6. Coefficients of the first level of non-decimated wavelet decomposition of the function Ang in Fig 5. Notice the behavior of the coefficients at $27°$, $90°$ and $119°$.

After analyzing real life images, an interesting feature is found: the peak at $90°$ almost always appears in the graph of the energy function Ang. It can be shown that this peak is an construct of the Hough transform. For instance, if Bernoulli random noise is used to create an original edge map image (with probability p for a given pixel to be 1), then the energy function Ang will have a distinct shape shown in Figure 7.

The sharpness of the peak depends on the percentage of ones in an edged map. Sometimes, some parts or the even a whole image will not posses any features of interest; still their energy function will have a distinctive shape as in Figure 7. Thus, the shape of the energy function of an image with only noise, can be used as a template function for the absence of linear structure in images. It is very unlikely that a realistic nanoscale image would have parallel lines at $90°$. Hence, peaks at $90°$ can be ignored.

After determining the orientation of the parallel lines, the next step is to find their location by analyzing the columns of the accumulator matrix R. The angles, which were found in the previous

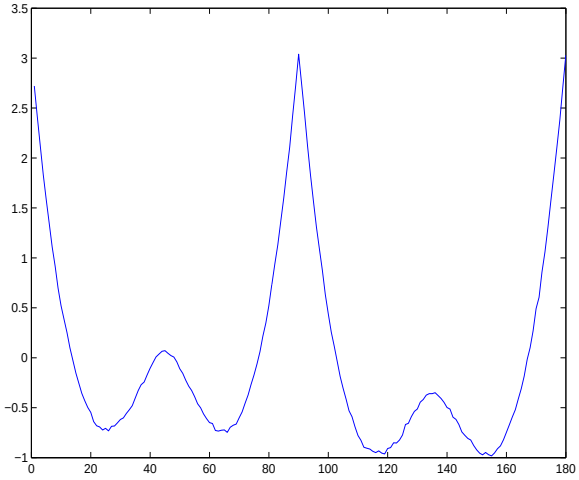

FIGURE 7. Function Ang that corresponds to the $0-1$ image with probability 0.1 for a given pixel to be 1.

step, would determine exactly which columns of the accumulator matrix are needed to be analyzed. For example, in the image in Figure 1 only two orientations were detected – one at 27° and a second at 119°. Therefore, one should focus on only the 27^{th} and 119^{th} columns of the matrix R. Figure 8 shows the 27^{th} column of the accumulator matrix R.

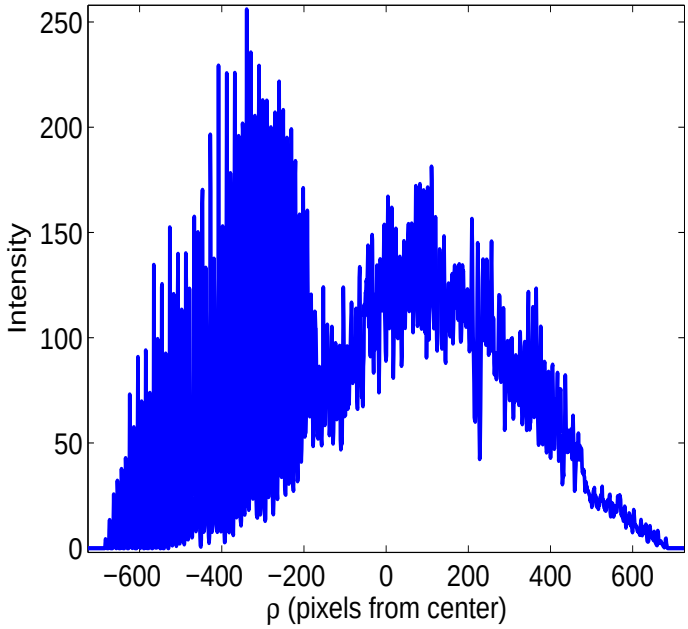

FIGURE 8. Plot of the 27^{th} column of the accumulator matrix R.

The relative thresholding will correspond to a horizontal cut on the graph in Figure 8. If the value of the threshold is too large (cut high) then too few lines would be detected. Lines that are close to the end of the image would be ignored, as well as the lines whose length is relatively small.

If the value of the threshold is too small (cut low), then too many "noise lines" would be detected which would be useless for the analysis. To this end, a compromising thresholding technique based on wavelets has been developed.

Let dis denote the column of interest of the accumulator matrix R. The length n of dis depends on the size of the original image. The signal dis is decomposed using a wavelet transform. The Vaidyanthan wavelet filter was selected for the decomposition. The sound-like form of the signals gives a strong indication that the Vaidyanathan wavelet is appropriate, since this filter has been optimized for speech coding. The number of levels in the wavelet decomposition is selected as

$$n_l = \left\lfloor \frac{\log_2(n-1)}{2} \right\rfloor. \tag{3}$$

The wavelet decomposition is thus composed of n_l levels containing the details of the signal dis, plus the smooth part, which contains the information about the general behavior of the signal. The number n_l as in the (3), ensures that the smooth part does not contain any high frequency features. Using only this smooth part of the wavelet decomposition, one can create a flexible threshold. Application of the inverse wavelet transform to the smooth part only produces the smoothed version of the signal dis. This reconstruction is used as a threshold criteria. The dotted curve in Figure 9 a) shows the smoothed signal dis. After shifting the restored signal by an appropriate constant, one can consider everything below the curve as insignificant. The standard deviation of the absolute values of the residuals of the signal dis and its restored smoothed representation is selected as the shift constant. The solid curve in Figure 9 a) represents shifted smoothed signal dis, which is used as a threshold. By itself this threshold is not selective enough, for it selects too many lines. The Vaidyanthan wavelet transform is then applied to the original signal dis again, but this time we ignore the first level (finest level) of the decomposition. Similarly, the inverse wavelet transform is applied to the smooth part of the decomposition. The restored signal repeats the behavior of the original signal dis almost perfectly. Figure 9 b) shows the restored signal with only one level of decomposition. There are key differences in a restored signal and the original signal which make it easier to eliminate most of the extra lines. The restored signal is based on only half of the data points of the original signal. It averages values of neighboring data points. The restored signal always shrinks towards its average. Everything below the restored signal is ignored. The combined two-step thresholding produces good results.

Another challenge comes from the pixel representation of a straight line. The granularity of the pixel representation of a line can be coarse enough for the Hough transform to detect two or more lines of the same orientation, where, in fact only one line exists (see Figure 10). Some orientations tend to create more neighboring parallel lines than the others. Experiments with different images have shown that orientations which favor generation of several lines are located in the neighborhood of the local minima of the function in Figure 7. This creates a problem for the analysis of the lattice spacing – the distance between parallel lines of the same direction. The introduction of several extra lines in close proximity will act as noise.

When working with real life images with visible linear structure, continuous straight lines are rarely found, since lines are broken into pieces. The lines are not always straight, due to the defects in a materials, and/or poor image quality. Thus, after edge detection there would be a noisy image with fragmented lines. Even in the continuous fragments of the same line one can observe small shifts (see Figure. 11). All these factors cause the single line to create several extra lines, which brings more noise into the analysis.

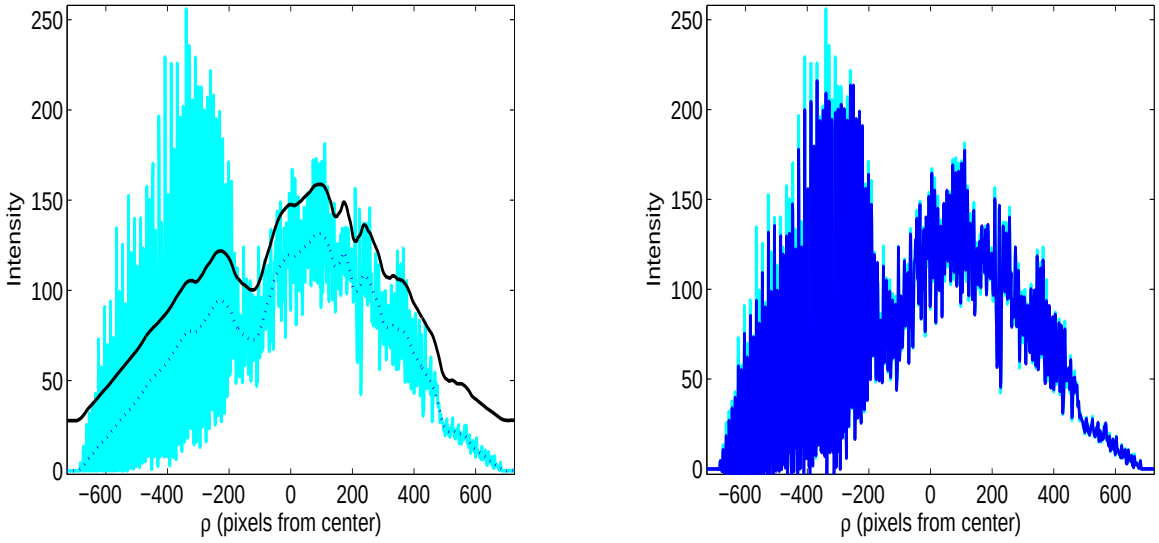

FIGURE 9. (a) Cyan - original signal. Dotted line - smoothed signal dis. Solid curve - shifted smoothed signal. (b) Cyan - original signal. Blue - restored signal without finest level.

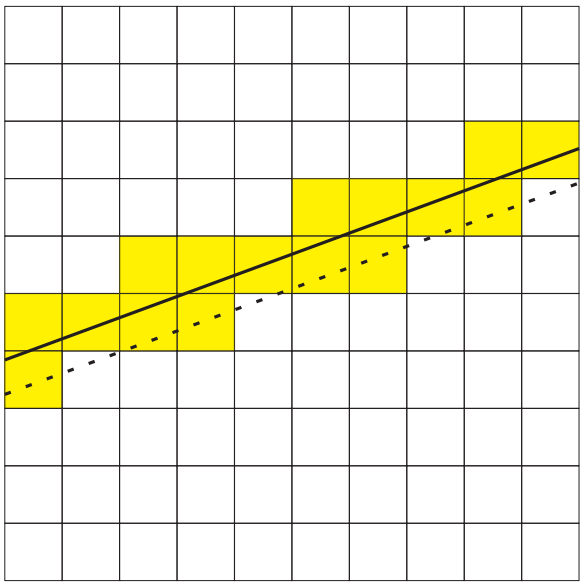

FIGURE 10. Theoretical line(solid); its pixel representation. The dotted lines represents a neighboring line, which might get detected since it goes through many pixels of the pixel representation.

The following procedure has been developed in order to solve this problem. Among detected lines, those that are one, two or three pixels apart were singled out. From the equations of these lines, pixel representations are generated. These representations are the coordinates of pixels outlining the original lines. Using these pixel coordinates the signal of zeros and ones can be obtained

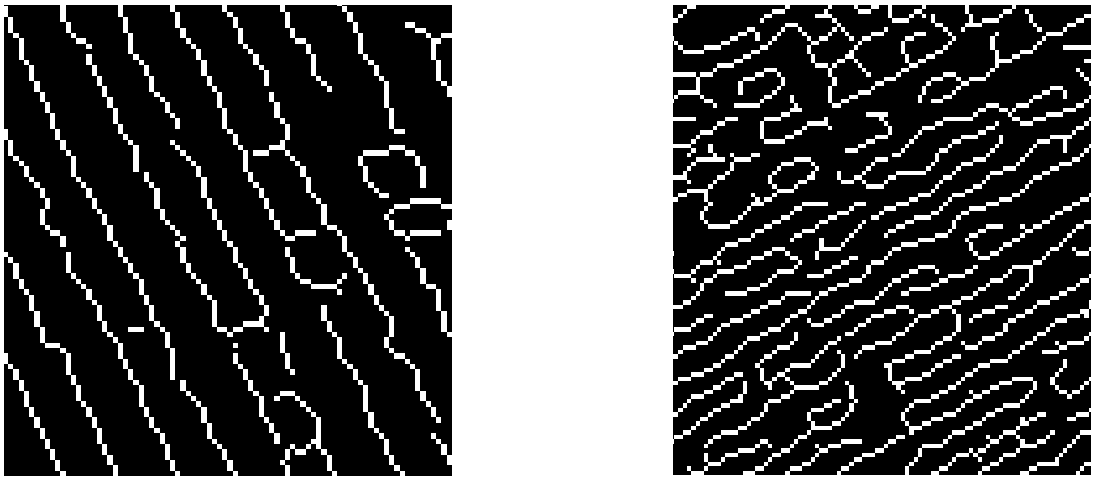

(a) (b)

FIGURE 11. A close-up on the linear structure of the ZnS structure. Notice how the lines formed by an atomic lattice are not exactly straight or continuous. One can clearly see that the lines are fragmented and continuous segments contain small shifts. All this generates problems in the analysis.

from the edge map, which would correspond to a line under investigation. One could choose several measurements in order to decide if the line is significant: the simple count of ones, the maximum length of the continuous run of ones, or the average length of runs of ones. The significance measure could help to differentiate between the actual line and the neighboring noise lines. Figure 12 illustrates the representation of a detected line and its neighbor. Clearly the second line b) is only detected because of the "spill-over" from line a). Therefore it could be ignored. This step improves the results significantly.

4. RESULTS

4.1. **Deterministic Images.** Several synthetic images of size 1024×1024 have been created in order to test performance of the method. All images consist of fifty parallel lines of various orientation with a fixed distance between them. Different levels of normal noise have been added to each image. Table 1 shows the results of the analysis of these images.
Notation: "# of lines" refers to number of lines detected. "Distance" denotes estimated average distance detected. "Std" refers to standard deviation of the estimated distance between the lines.
Since all the lines have a fixed distance between them, standard deviation theoretically should be zero. However, because of approximations in constructing lines (i.e. pixel representation) some small variability is expected. Images 1 through 4 have single orientation, where images 5-7 have two sets of parallel lines and image 8 has three. Figure 13 shows an enlarged portion of image 8 together with the noise added to this image.

4.2. **Nanoscale Images.** Application of the method is demonstrated on the two TEM images of the ZnS structures. Figures 14 and 15 show the images. Because of their large size the images

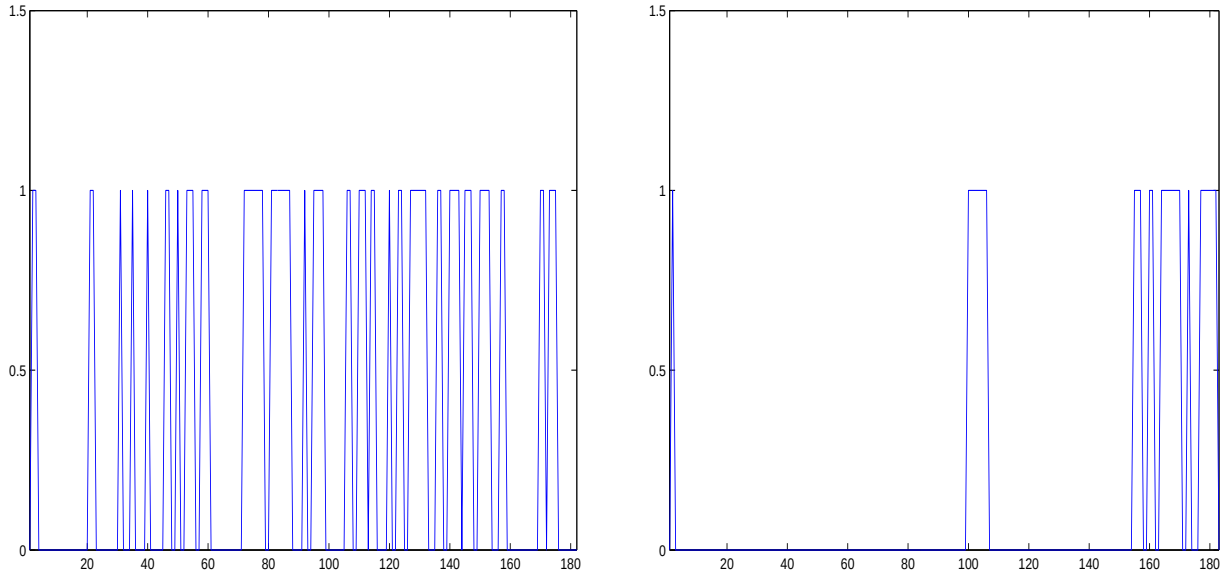

(a) (b)

FIGURE 12. Representation of the two neighboring lines detected after thresholding. Line (b) is clearly detected as a "spill-over" from line (a) and can be ignored.

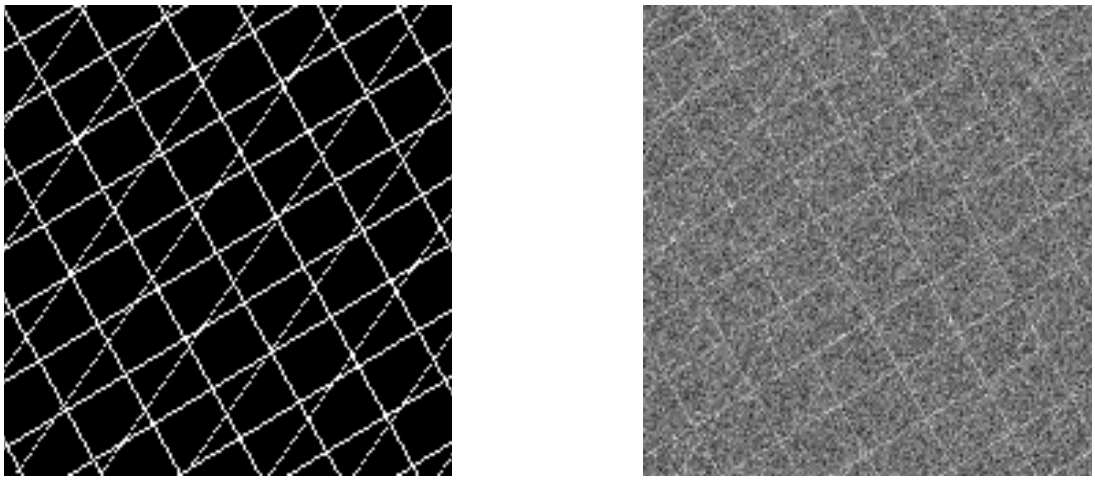

(a) (b)

FIGURE 13. (a) Example of the deterministic image with three sets of parallel lines; (b) Example of the deterministic image with added normal noise (SNR=0.5). Notice how the lines with 144° orientation are barely visible in the noise.

have been broken into 4 subimages in the following manner $\begin{array}{|c|c|}\hline (1,1) & (1,2) \\ \hline (2,1) & (2,2) \\ \hline \end{array}$. Each subimage is analyzed separately. The results for each image can be found in Tables 2-4. The results are given for the default parameter settings, using three-pixel difference elimination for close lines. A 10%

Description	SNR	0.3	0.5	0.7	1	3	No Noise
Image 1(1 set)	# of lines	51	49	49	49	49	49
Distance between the lines is 25 pixels	Distance	23.5	25.06	24.93	25	25	25
Angle 30° between lines and y axis	Std	4.445	1.31	1.31	0.87	5.80E-15	5.86E-15
Image 2(1 set)	# of lines	66	47	47	47	49	49
Distance between the lines is 20 pixels	Distance	16.18	20.06	20	20	19.58	20
Angle 150° between lines and y axis	Std	10.2	2.4	2	2	2.5	1.60E-14
Image 3(1 set)	# of lines	49	49	48	48	48	48
Distance between the lines is 20 pixels	Distance	19.58	20	20	20	20	20
Angle 120° between lines and y axis	Std	3.03	1.23	0.437	1.25	8.38E-15	8.38E-15
Image 4(1 set)	# of lines	67	50	48	46	47	48
Distance between the lines is 25 pixels	Distance	17.42	24.42	25	25	24.93	25
Angle 144° between lines and y axis	Std	8.29	5.26	1.37	1.73	1.18	1.67E-15
Image 5(2 sets) Set 1:	# of lines	70	49	49	49	49	49
Distance between the lines is 25 pixels	Distance	17.75	25.06	24.93	25	24.93	25
Angle 30° between lines and y axis	Std	7.25	1.15	1.31	1.07	1.8	1.51
Set 2:	# of lines	117	64	50	49	49	49
Distance between the lines is 25 pixels	Distance	10.9	19	24	25.06	25	25
Angle 144° between lines and y axis	Std	6.16	7.49	4.38	1.42	0.41	0.41
Image 6(2 sets) Set 1:	# of lines	86	51	49	49	49	49
Distance between the lines is 25 pixels	Distance	14.21	24.44	25	24.93	25	25
Angle 30° between lines and y axis	Std	6.95	2.84	1.23	0.97	1.51	2.55
Set 2:	# of lines	73	49	48	48	48	49
Distance between the lines is 20 pixels	Distance	15.36	20	20	20	20	19.93
Angle 120° between lines and y axis	Std	11.3	1.75	1.39	0.625	1.97	1.57
Image 7(2 sets) Set 1:	# of lines	66	49	49	49	49	49
Distance between the lines is 20 pixels	Distance	16.09	19.93	20	20	20	20
Angle 120° between lines and y axis	Std	6.95	1.64	1.23	8.23E-15	8.29E-15	8.29E-15
Set 2:	# of lines	119	72	50	50	49	49
Distance between the lines is 25 pixels	Distance	10.4	16.95	24.53	25.04	25	24.97
Angle 144° between lines and y axis	Std	5.83	7.65	2.78	1.15	0.61	0.14
Image 8(3 sets) Set 1:	# of lines	98	52	48	49	49	49
Distance between the lines is 25 pixels	Distance	12.53	24.07	25	25	25	25.06
Angle 30° between lines and y axis	Std	6.66	3.74	1.25	1.51	1.51	2.18
Set 2:	# of lines	89	51	49	49	49	49
Distance between the lines is 20 pixels	Distance	14.02	19.54	20.06	19.93	20	20
Angle 120° between lines and y axis	Std	10.35	2.71	1.57	1.15	8.29E-15	8.29E-15
Set 3:	# of lines	Failed	107	55	50	50	51
Distance between the lines is 25 pixels	Distance		11.94	22.18	25	24.95	24.52
Angle 144° between lines and y axis	Std		6.8	5.63	1.25	0.28	2.97

TABLE 1. Analysis of the deterministic images. Each set of lines consists of 50 parallel lines.

trimming from above is applied, for the estimation of the average distance between parallel lines or lattice spacing. The theoretical lattice spacing for the ZnS materials is $1.66 \cdot 10^{-10}$ m. This if for the inside of material in ideal condition, as on the surface the spacing may vary. As one can see from the Tables 2-4, the estimate of the major layer is almost always greater than the theoretical

distance. However, the estimate of distances for visible layers under the surface is very close to the theoretical distance.

On the surface, the atoms experience different energetic responses than in the bulk of the material. In order to compensate, the atomic layer relaxes (spreads out) or otherwise rearranges itself. This is the major reason why the estimated distance of the main visible layer exceeds the theoretical distance. For some of the materials the way atoms rearrange themselves on the surface is well studied, and the lattice spacing could be determined theoretically. For the others there is no method that would give good understanding of the rearrangements and provide theoretical lattice spacing. Our method allows the experimenter to estimate the lattice spacings quite accurately.

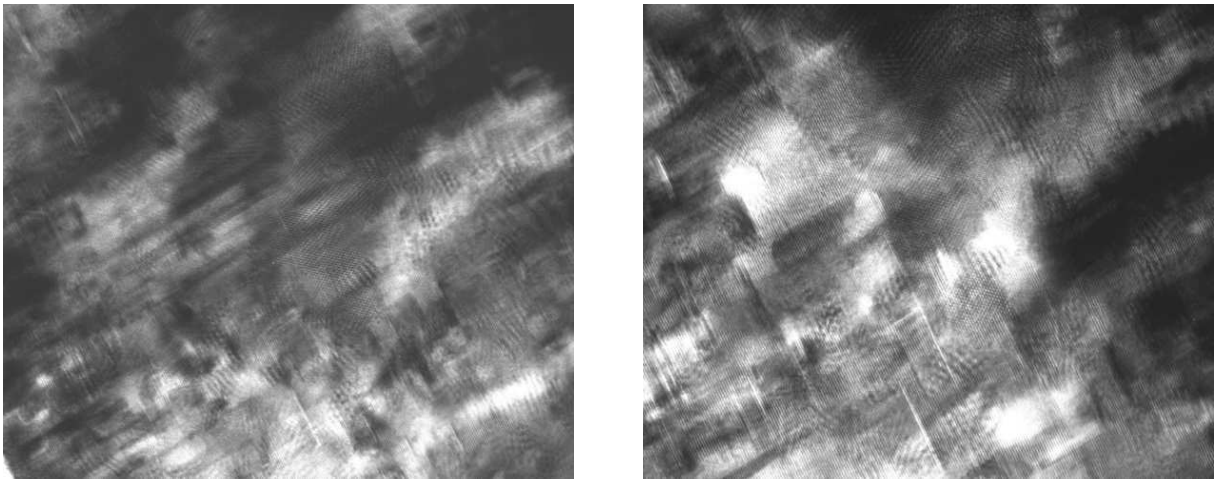

(a) (b)

FIGURE 14. (a) Image 1: size 4050×5220; (b) Image 2: size 3360×4560.

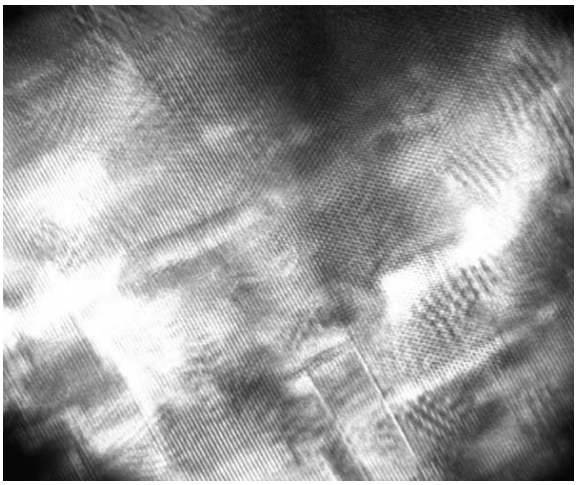

FIGURE 15. Image 3: size 2415×2745.

4.3. **Image 1.** Size 4050×5220, scanned at 2400dpi and with microscope magnification of 500,000. The image is broken into 4(2x2) overlapping images 2048×2048, which give almost complete

coverage of the original image. Quality of the subimage (1, 2) is poor. No features are found with default parameter settings. Results of the analysis are in Table 2. 29° is the major visible orientation present almost throughout the entire image. 78° is visible only in part of the image.

Subimage	Detected Direction	Average(in m.)
(1, 1)	29	2.18E-10
(2, 1)	29	2.37E-10
(2, 2)	29	2.16E-10
	78	2.49E-10

TABLE 2. Image 1 analysis.

4.4. **Image 2.** Size 3360×4560, scanned at 2400dpi and with microscope magnification of 500,000. The image is been broken into 4(2x2) overlapping images 2048×2048, which give almost complete coverage of the original image. 28° is the major visible orientation present almost throughout the entire image. 118° is the secondary orientation present almost always throughout the whole image, but is barely visible, and with default parameter it is detected only once. Results of the analysis are in Table 3.

Subimage	Detected Direction	Average(in m.)
(1, 1)	28	2.03E-10
(1, 2)	28	2.03E-10
	99	2.10E-10
(2, 1)	28	2.06E-10
(2, 2)	28	2.10E-10
	118	1.71E-10

TABLE 3. Image 2 analysis.

4.5. **Image 3.** Size 2415×2745, 2400dpi and with microscope magnification of 500,000 times. The image is broken into 4(2x2) overlapping images 2048×2048, which give complete coverage of the original image. Results of the analysis are in Table 4.

Subimage	Detected Direction	Average(in m.)
(1, 1)	28	2.03E-10
(1, 2)	28	2.06E-10
	118	1.89E-10
(2, 1)	28	2.03E-10
(2, 2)	28	2.30E-10
	100	1.73E-10
	118	1.81E-10

TABLE 4. Image 3 analysis.

5. Conclusions and Discussion

In this paper we propose a new method for the analysis of the nanoscale images. The proposed method produces good results in both synthetic and real nano-scale images. It is recommended to have two images of the same sample: one the rotated version of the other. Comparison of the results of both images would allow for the removal of the uncertainty that comes from the sensitivity of the Hough transform to certain orientations. This would increase accuracy in the analysis of the lattice spacing. Current 'algorithmic' methods of image rotation would preserve the image's structure completely, and the energy function would shift according to the angle of rotation (see Figure 16). This is why it is recommended to have two images.

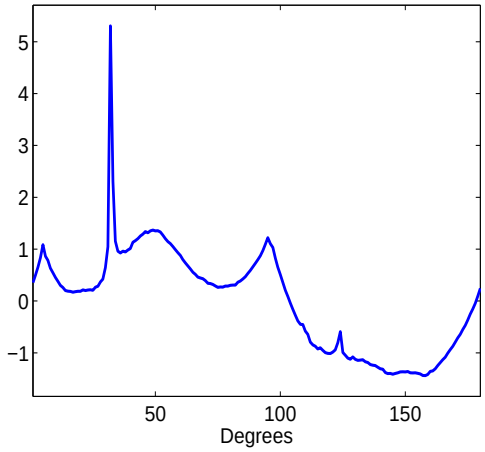

FIGURE 16. Plot of the energy function of the rotated by 5° image. The energy function of the rotated image almost completely preserves structure of the energy function for the original image. Everything is shifted by 5°.

It is possible to perform continuous directional wavelet transform of the images with the directions defined by the output of the analysis. The continuous directional wavelet transform would extract the features of the images which are aligned in the given direction. Figure 17 shows the continuous directional wavelet transform of the image in Figure 1 in two directions 27° and 119°. The results of the continuous directional wavelet transform could tell a little bit more about structure and defects in the material for specific orientation.

We support David Donoho's initiative for reproducible research. MATLAB toolbox, tutorial file, sample images, and m-files used to produce the calculations and pictures in this paper are available at Jacket's Wavelets page `http://www.isye.gatech.edu/~brani/wavelet.html`.

References

[1] Deans S.R., *Hough Transform From the Radon Transform*, IEEE Trans. Pattern Analysis and Machine Intelligence, PAMI-3(2) March 1981.

[2] Duda R.O., and Hart P.E., *Use of the Hough Transform to Detect Lines and Curves in Pictures*, Comm ACM 15, pp 11-15, January 1972.

[3] Hough P.V.C., *Method and Means for Recognizing Complex Patterns*, U.S. Patent No. 3069654, 1962.

[4] Illigworth J. and Kittler J., *A Survey of the Hough Transform*, Computer Vision Graphics and Image Processing, 44, pp 87-116, 1988.

[5] Leavers V.F., *Shape detection is Computer Vision Using the Hough Transform*, Springer-Verlag, 1992.

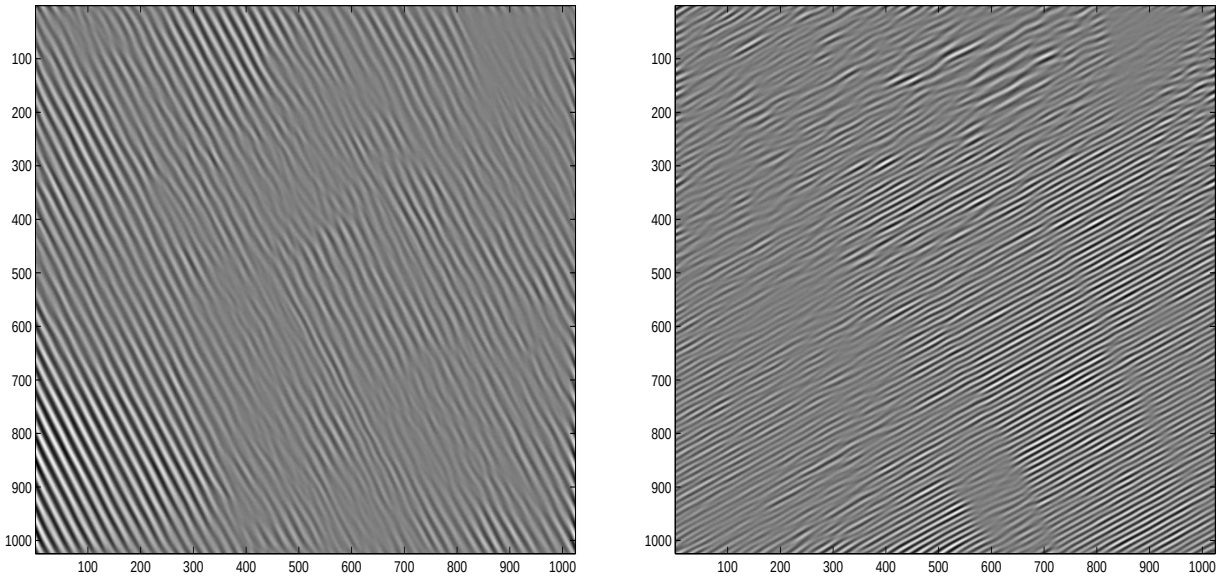

FIGURE 17. Continuous Direction Wavelet Transforms of image in Fig. 1 a) 27° b) 119°.

[6] Magli E., Olmo G., *Integrated Compression and Linear Feature Detection in the Wavelet Domain*, ICIP 2000 – IEEE International Conference on Image Processing, Vancuver, Canada 2000.
[7] Vidakovic B., *Statistical Modeling by Wavelets*, New York: John Wiley & Sons, 1999.

(Ilya Lavrik and Brani Vidakovic) INDUSTRIAL AND SYSTEM ENGINEERING, GEORGIA INSTITUTE OF TECHNOLOGY, ATLANTA, GEORGIA 30332-0205, USA.

E-mail address, Ilya Lavrik: ilavrik@isye.gatech.edu

E-mail address, Brani Vidakovic: brani@isye.gatech.edu